INTERNATIONAL SOCIETY FOR SOIL MECHANICS AND GEOTECHNICAL ENGINEERING



This paper was downloaded from the Online Library of the International Society for Soil Mechanics and Geotechnical Engineering (ISSMGE). The library is available here:

https://www.issmge.org/publications/online-library

This is an open-access database that archives thousands of papers published under the Auspices of the ISSMGE and maintained by the Innovation and Development Committee of ISSMGE.

The paper was published in the proceedings of the 20th International Conference on Soil Mechanics and Geotechnical Engineering and was edited by Mizanur Rahman and Mark Jaksa. The conference was held from May 1st to May 5th 2022 in Sydney, Australia.

Particle-scale simulation of drained cyclic loading of sand at a constant mean effective stress

Effets de chargements cycliques drainés avec une contrainte effective moyenne constante sur le sable.

Tara Sassel & Catherine O'Sullivan

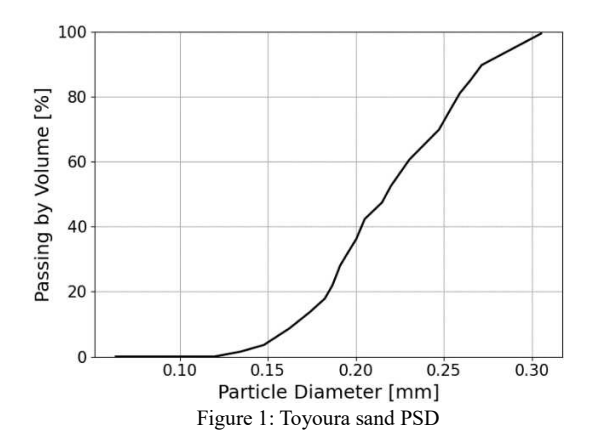
Department of Civil and Environmental Engineering, Imperial College London, SW7 2AZ London, UK, tara.sassel17@ic.ac.uk

ABSTRACT: The discrete element method (DEM) was used to simulate drained cyclic loading of cubical samples of spheres with a particle size distribution similar to Toyoura sand. The samples were compressed at a range of mean effective stresses and subsequently subjected to drained cyclic loading at different amplitudes maintaining a constant mean effective stress. The relationships between axial, volumetric shear and deviatoric strain during cyclic loading are explored. The evolution of both frictional and strain energy as well as the coordination number are considered.

RÉSUMÉ: La méthode aux éléments discrets a été utilisée pour conduire des chargements cycliques drainés sur des échantillons cubiques de sphères avec une distribution granulométrique similaire à celui du sable de Toyoura. Les échantillons ont alors été compressés à une rangée de contraintes effectives moyenne. Ensuite, les échantillons ont été chargés cycliquement avec des amplitudes différentes tout en maintenant une contrainte effective moyenne constante. Les relations entre les déformations axiales, volumétriques, de cisaillement et déviatoriques découlant de charges cycliques sont étudiées. Le changement en énergie de friction et de déformation ainsi que le nombre de contacts par particule sont considérés. (contrainte effective moyenne constante, méthode aux éléments discrètes, chargement cyclique drainé, sable)

KEYWORDS: constant mean effective stress, DEM, drained cyclic loading, sand

1 INTRODUCTION



Cyclic loading at low amplitudes is often observed adjacent to structures such as wind turbines with monopile foundations and integral bridge abutments. According to Wichtmann et al. (2005) these cyclic loads / deformations occur under drained conditions and have a strain amplitude $\varepsilon^{ampl} < 10^{-3}$. Where there are a high number of load cycles there can be an accumulation of strain leading to settlement. This accumulation of strains is irreversible and also known as ratcheting. Kohadir (2009) assumed that ratcheting occurs because the soil has a softer response during reloading in comparison to the response during unloading and that this is associated with a change in soil fabric/a rearrangement of particles during unloading. Several constitutive models have been developed to predict ratcheting (these include viscoplastic models described in Chaboche and Nouailhas (1989) and the HARM model by Houlsby et al. (2017)). The evolution of fabric and particle rearrangements cannot be captured in the constitutive models used in FEM. DEM helps us to monitor these changes and examine the fundamental mechanism for ratcheting. Thornton (2000) showed that DEM can be used to carry out triaxial tests on granular materials such as sands and that their stress-strain behavior can be captured when using periodic boundaries. Huang et al. (2014) demonstrated that when using a representative soil grading with a representative number of particles, the position of the critical state line (CSL) can be determined.

DEM simulations enable us to relate the macroscopic to the microscopic scale. The objectives of this study are to relate the macroscopic behavior during cyclic loading, i.e. the evolution in volumetric strain, to the particle-scale behavior by considering appropriate metrics including the coordination number.

2 TEST PROCEDURE AND RESULTS

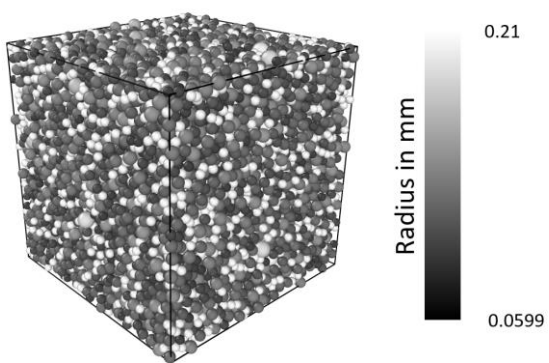


Figure 2: DEM sample with particles colored by radius

Using the DEM code granular LAMMPS (Plimpton, 1995) a sample with the particle size distribution (PSD) of Toyoura sand was generated as shown in Figure 1. The sample of 19,463 particles which is shown in Figure 2 was encased within periodic boundaries. The contact model that was used for these

simulations was the Hertz-Mindlin model (Hertz, 1981). This model captures the stress dependency of the stiffness of the contacts between particles that occur in physical systems. The simplified Hertz-Mindlin model implemented here has been used in prior soil mechanics studies; notably Huang et al. (2014) found quantitative agreement between simulations using this model and experimental data from Jefferies and Been (2006). O'Sullivan et al. (2008) directly compared DEM data with experiments on ideal spheres and showed that the cyclic response could be accurately captured.

For these simulations a shear modulus G' of 29.17GPa and a Poisson's ratio v = 0.2 were used. The particles were assigned an interparticle friction coefficient of 0.25.

Initially a non-contacting cloud of particles was generated using an in-house particle generation script that ensures homogeneity within the sample. Following generation, the sample was isotopically compressed using servo-controlled boundaries to mean effective stresses of p_0' equal to 100, 200 or 300 kPa. Each sample was then subject to cyclic loading where the axial stress, σ'_{zz} , varied according to the amplitude +/- σ'^{ampl} . During loading the mean effective stress p' was maintained constant so that the lateral effective stresses σ'_{xx} and σ'_{yy} varied. Representative stress data for a sample loaded at p' = 200 kPa and $\sigma'^{ampl} = +/-20 k$ Pa are shown in Figure 3.

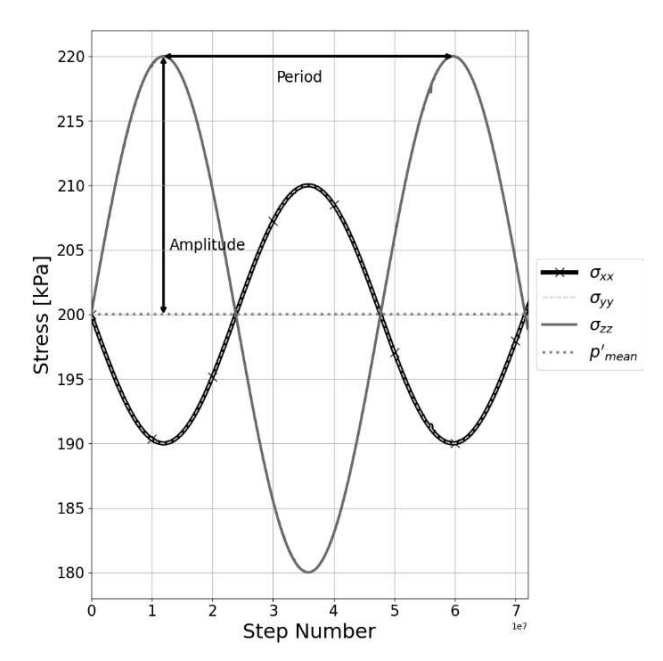


Figure 3: Cyclic loading of sample

2.1 Effect of drained cyclic loading on volumetric strains

Figure 4 presents data for three tests with p'=100, 200 and 300kPa. In each case the axial stress is plotted against the volumetric strain ε_v . For all of these tests the ratio of load amplitude to p', $\zeta=q^{ampl}/p'$, is 0.1.

Referring to Figure 4 (a), for the lowest p' (=100kPa) it took 8 cycles to reach $\varepsilon_v = 0.25\%$, whereas it took 18 and 23 cycles to reach $\varepsilon_v = 0.25\%$, when p' = 200kPa and 300kPa respectively (Figure 4 (b) and (c)). In all cases there is a decrease in the increment in volumetric strain over each cycle with increasing cycle number. The smallest increments are observed for the lowest mean effective stress. This accumulation in volumetric strain is permanent.

This reduction in the per-cycle strain increment is related to the ratcheting phenomenon mentioned above. This softer response during reloading is apparent in our data sets especially as the number of cycles increase. The increase in ε_{ν} is more

significant as σ'_{zz} increases from its minimum to its maximum value than the reduction in ε_v during unloading from the maximum σ'_{zz} to the minimum σ'_{zz} .

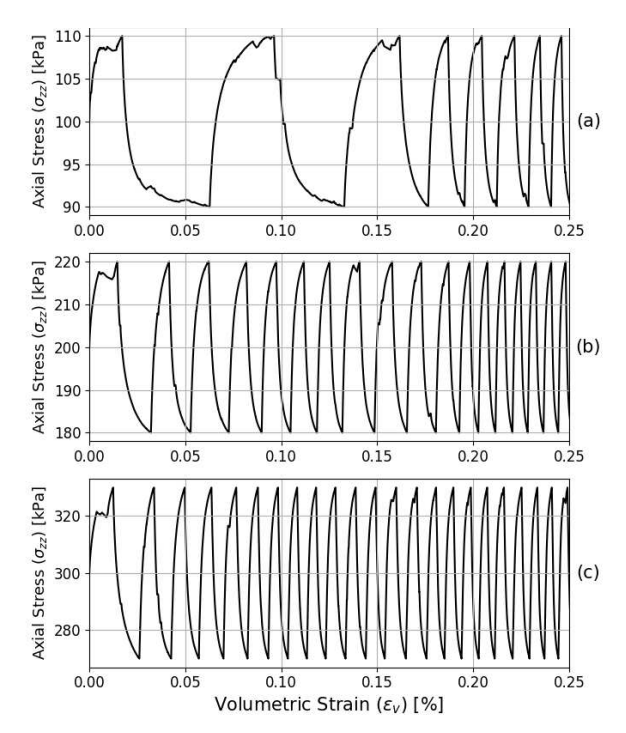


Figure 4: Axial stress vs volumetric stress for p_0 ' = 100 (a), 200 (b) and 300kPa (c) at $\zeta = 0.1$

2.2 Effect of drained cyclic loading on axial strain amplitudes

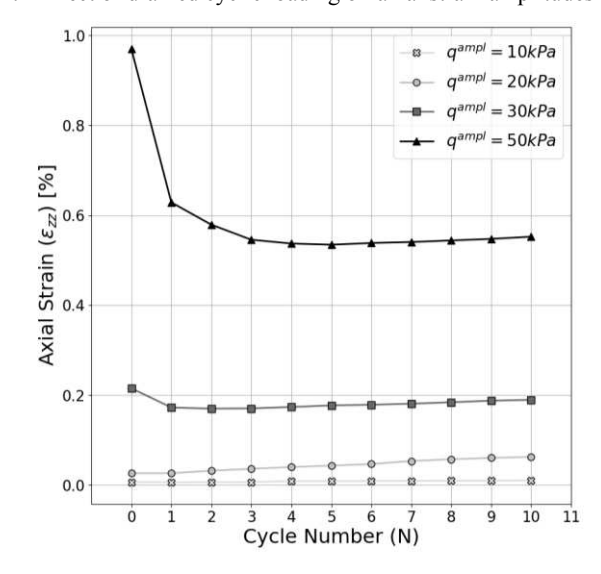


Figure 5: Axial strain at maxima's against cycle number for p' = 200kPa at different amplitudes

Four test simulations were carried out at constant p' values of both 200 kPa and 300 kPa where the applied stress amplitudes were between 10kPa $\leq q^{ampl} \leq 50$ kPa.

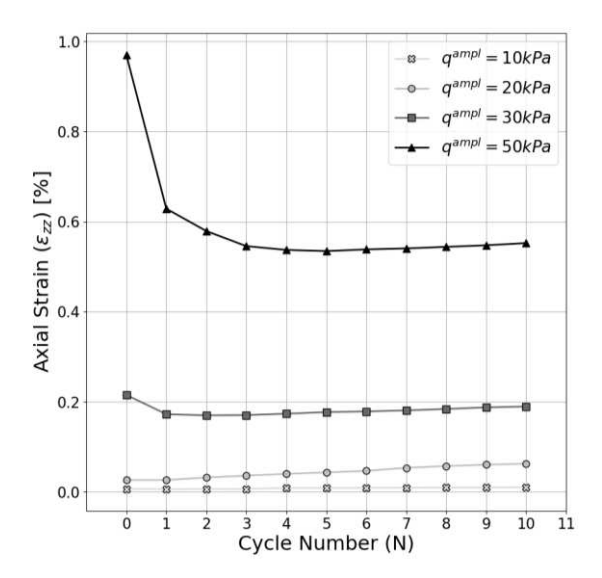


Figure 5: Axial strain at maxima's against cycle number for p' = 200kPa at different amplitudes

and Error! Reference source not found. consider the axial strain amplitude ε_{zz}^{ampl} by plotting the maximum ε_{zz}^{ampl} for each cycle against the cycle number. Where p'=200kPa (Figure 5), a marked decrease in ε_{zz}^{ampl} can be observed for the highest amplitude q^{ampl} of 50 kPa over the initial cycles (N=5) followed by a slight increase. A similar trend was observed for p'=300kPa and $q^{ampl}=50$ kPa (Figure 6); however, the decrease occurred only over the first two cycles and the subsequent increase in ε_{zz}^{ampl} was larger. For both p'=200kPa and p'=300kPa an increase in ε_{zz}^{ampl} could already be observed after the first cycle for $q^{ampl}=10$, 20 and 30kPa. These observations are in accordance with Wichtmann et al. (2005, 2007).

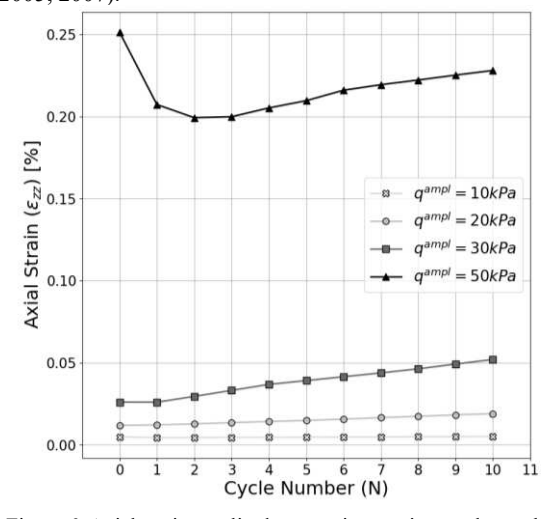


Figure 6: Axial strain amplitude at maxima against cycle number for p' = 300kPa at different amplitudes

Error! Reference source not found. considers the axial strain (ε_{zz}) at three characteristic reference points during cyclic loading for $\zeta = 0.1$ and $p_0' = 100$, 200 & 300 kPa. The first point is where $q = q_{zero}$ before loading, which is at the start of each cycle. The two other points are at the local maxima $q = +q^{ampl}$ and the local minima $q = -q^{ampl}$.

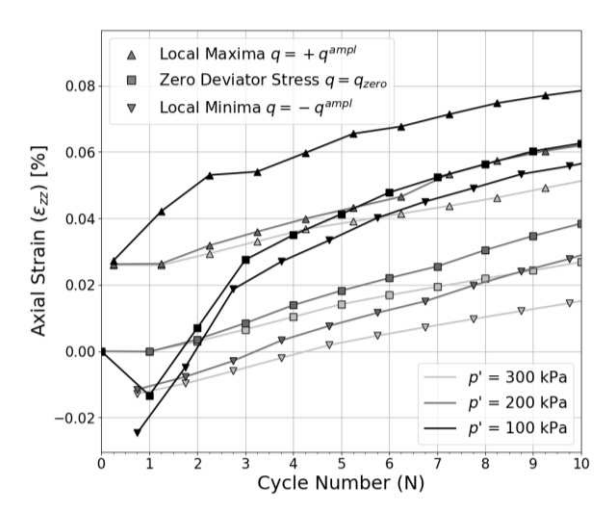


Figure 7: Axial strain vs cycle number N for different p' for $\zeta = 0.1$

An increase in axial strain can be noted at all key positions and the most noticeable increase can be observed for the lowest p' of 100kPa. The magnitude of the increment decreases with p' and the slope of the lines is roughly the same for the three loading positions.

In **Error! Reference source not found.** the strain at the maxima over the first 10 cycles are plotted against the deviatoric stress amplitude q^{ampl} . The strains that are plotted are the axial strain ε_{zz} , the volumetric strain ε_v and the deviatoric strain ε_q . ε_v and ε_q are defined as in Wood (1990):

$$\varepsilon_q = \frac{2}{3} \left(\varepsilon_{zz} - 0.5 \left(\varepsilon_{xx} + \varepsilon_{yy} \right) \right)$$
 (1)

$$\varepsilon_{v} = \varepsilon_{xx} + \varepsilon_{yy} + \varepsilon_{zz}$$
 (2)

In Error! Reference source not found. an increase in ε_{zz} , ε_q and ε_v can be observed with increasing deviatoric stress amplitude. The increase in axial and volumetric strain is not linear rather it appears to triple when q^{ampl} is doubled. ε_v is increasing the fastest and ε_q the least which can be related to the nature of equation (1) and (2) where all total strains $(\varepsilon_{xx}, \varepsilon_{yy}, \varepsilon_{zz})$ are positive.

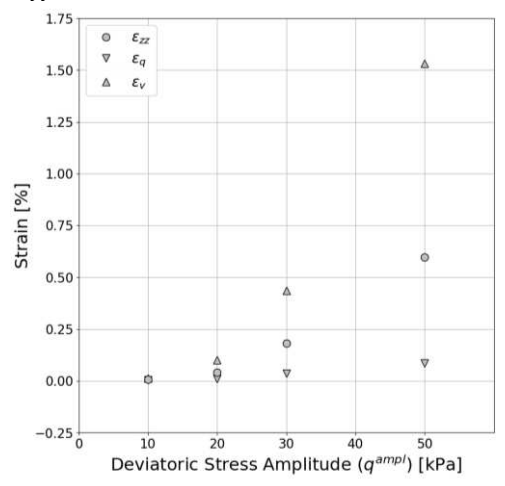


Figure 8: Strain against the deviatoric stress amplitude q^{ampl} at p' = 200kPa

In Figure 9 the average strain at the maxima over the first 10 cycles are plotted against the effective mean stress p' at $\zeta=0.1$ meaning that for p' of 100, 200 and 300 kPa q^{ampl} are 10, 20 and 30 kPa respectively. Again, an increase in deviatoric strain can

be observed similar to the data in Wichtmann et al. (2005) and (2007). Additionally, a clear decrease in axial and volumetric strain can be observed with increase in p'. This decrease can be explained by referring to

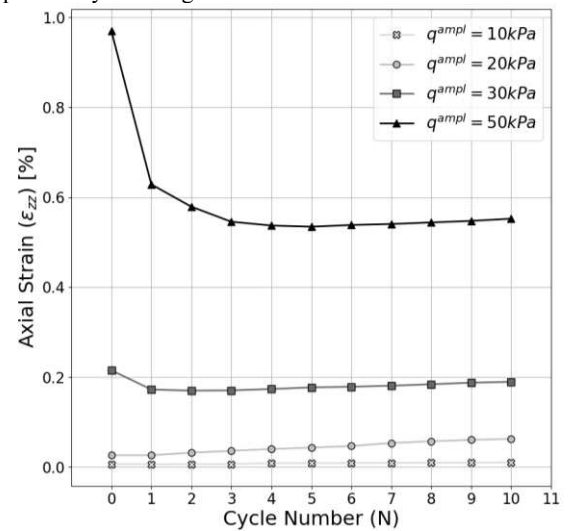


Figure 5: Axial strain at maxima's against cycle number for p' = 200kPa at different amplitudes

, as only 10 cycles are taken into account for each case the average of the sum of the first 10 peaks is much higher for a mean effective stress of 100kPa.

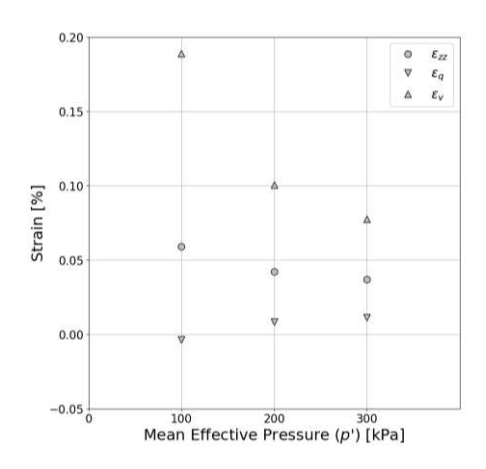


Figure 9: Average strain at maxima over first 10 cycles against the average mean pressure p' for $\zeta=0.1$

2.3 Effect of drained cyclic loading on coordination number

The coordination number is the number of contacts per particle and therefore is a measure of packing density:

$$Z = \frac{2N_c}{N_n} \tag{3}$$

where N_c is the number of contacts and N_p is the number of particles. As one contact is shared between two particles this number has to be multiplied by two. In Figure 10 the coordination number when ε_{zz} is at the maxima for each cycle is plotted against cycle number for $\zeta=0.1$. As can reasonably be expected Z increases with increasing p'. For p'=200 and $300\text{kPa}\ Z$ at this characteristic point decreases very slightly with N; arguably evidence of a systematic reduction in Z is not at all clear for p'=200 kPa. There is an increase in Z with N for the sample with p'=100 kPa. However, no clear trend can be deduced considering all three stress levels.

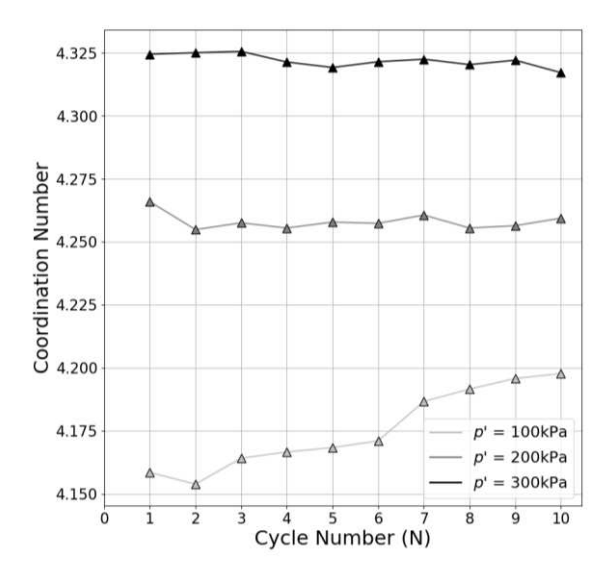


Figure 10: Coordination number against cycle number for $\zeta = 0.1$

2.4 Energy dissipation

As the slope of the load deformation responses in loading and unloading differ there is clearly energy dissipation during the cyclic loading scenarios considered here. Using DEM the frictional energy E_f^β dissipated in the system up to timestep β can be calculated. E_f^β is a cumulative sum; at each timestep β the sum of the change in frictional energy at each contact $\sum_{j=i}^{N_c} \delta E_f^{\beta-1}$ is added to the frictional energy at the previous timestep $E_f^{\beta-1}$ (Keishing et al., 2020):

$$E_f^{\beta} = E_f^{\beta - 1} + \sum_{j=i}^{N_c} \delta E_{f_j}^{\beta - 1} \tag{4}$$

In Figure 11 the frictional energy dissipated is plotted against ε_{zz} ; cycles N=1 and 20 are illustrated in gray and the data for these cycles are shown in more detail in the two subplots. The frictional energy always increases because it is calculated cumulatively and is irreversible. The frictional energy dissipated in cycle 1 is about 0.014×10^{-3} J. The amount of frictional energy dissipated in each cycle decreases with increasing cycle number. At cycle number 20, the increase in frictional energy is 0.004×10^{-3} J. Similar trends could be observed for all other data sets independent of mean effective stress or amplitude.

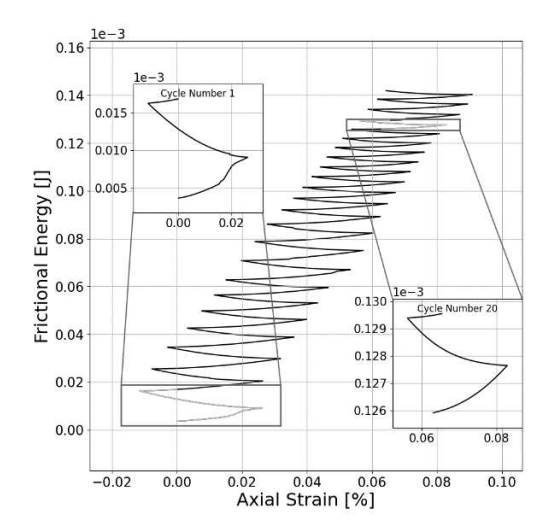


Figure 11: Frictional energy against axial strain p' = 200kPa and $\zeta = 0.1$

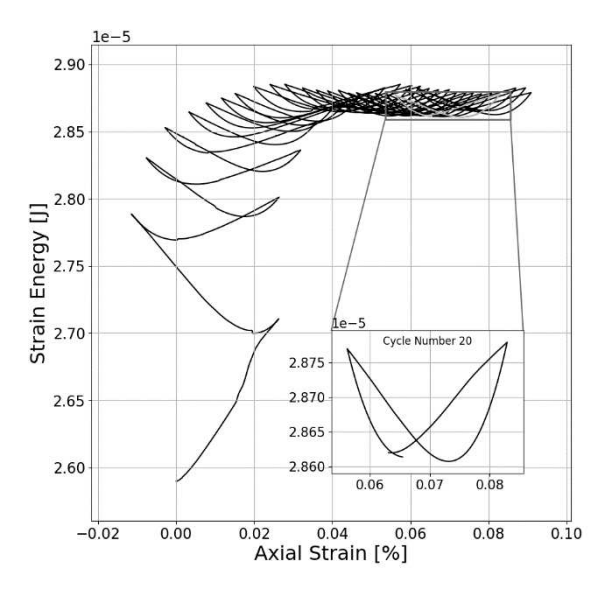


Figure 12: Strain energy against axial strain p' = 200kPa and $\zeta = 0.1$

The total normal and tangential strain energy are found by summation over all particle contacts $N_{\rm c}$. The tangential component is calculated incrementally. In both cases these strain energies calculated by considering the area under the relevant force: displacement plot for each contact.

Figure 12 considers the variation in total strain energy which is the sum of the normal and tangential strain energy with ε_{zz} , cycle 20 is indicated in gray and included in the subplot. The variation in strain energy in each cycle is consistently described by a butterfly-type shape after a about 10 cycles where the strain energy is non-dissipative.

In Figure 13 the strain energy is plotted against the axial strain at p'=300 kPa. The effect of different ratios of loading amplitude is compared. For $\zeta < 0.1$ there was an increase in strain following a similar trend to the frictional energy (Figure 13(a)). From Figure 13 (b) and (c) it can be observed that for a mean effective stress of 300kPa at $\zeta \geq 0.1$ the strain energy loop followed the same path at cycle numbers that are higher than 5. However, the strain energy decreases for $\zeta > 0.1$ until it seems to level off.

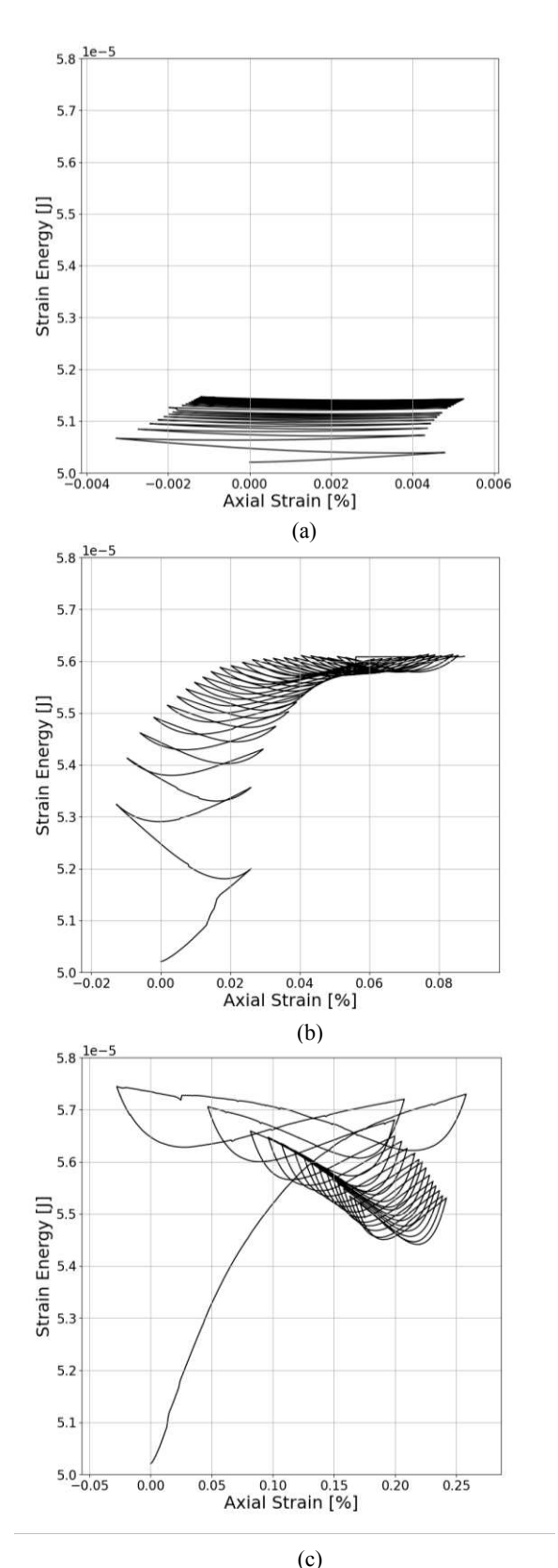


Figure 13: Strain energy against axial strain for p' = 300kPa where (a) $\zeta < 0.1$ q^{ampl} = 10 kPa (b) $\zeta = 0.1$ q^{ampl} = 30 kPa (c) $\zeta > 0.1$ q^{ampl} = 50 kPa

3 CONCLUSIONS

This contribution has presented data from DEM simulations of drained stress-controlled cyclic triaxial simulations carried out at mean effective stresses p' (100, 200 and 300kPa) and with deviatoric stress amplitudes of 10, 20, 30 and 50kPa. This paper demonstrates that:

- DEM can capture key elements of response to drained cyclic loading, including the accumulation of permanent in volumetric strain. The ratcheting rate decreases as the confining pressure increases.
- (2) At higher amplitudes, an initial decrease in ε_{zz} can be observed followed by an increase. This initial decrease is more significant at a smaller p'.
- (3) There was no significant variation in coordination number with cyclic loading.
- (4) An increase in frictional energy per cycle at a decreasing rate can be observed independent of the mean effective stress or the amplitude.
- (5) The pattern of strain energy variation depends on the loading amplitude ratio, ζ.

4 ACKNOWLEDGEMENTS

This work used the HPC facilities at Imperial College London. The first authors project is part of the CDT in Civil and Environmental Engineering at Imperial College London.

5 REFERENCES

- Chaboche, J.L. and Nouaihas, D. (1989) Constitutive Modeling of Ratchetting Effects Part I: Experimental Facts and Properties of the Classical Models. *Journal of Engineering Materials and Technology* 111 (4), 384-392.
- Houlsby, G.T. et al. (2017) A model for nonlinear hysteretic and ratcheting behavior. *International Journal of Soils and Structures*. 120 (1), 67 80.
- Huang X., Hanely K.J., O'Sullivan C. & Kwok F.C.Y. (2014) Effect of sample size on the response of DEM samples with a realistic grading. Particuology 15, 107 – 115.
- Jefferies M. and Been K. (2006) Soil liquefaction: a critical state approach, Taylor & Francis, New York.
- Keishing, J., Huang, X. & Hanley, K. (2020), Energy dissipation in soil samples during cyclic triaxial simulations, Computers and Géotechnics 121, 103481.
- Khodair, Y. A. (2009) Lateral earth pressure behind an integral abutment. Structure and Infrastructure Engineering 5(2), 123-136.
- O'Sullivan, C., Cui, L., and O'Neill, S. C. (2008) Discrete element analysis of the response of granular materials during cyclic loading Soils and Foundations 48 (4), 511-530
- Plimpton S. (1995) Fast Parallel Algorithms for Short-Range Molecular Dynamics. *Journal of computational physics* 117, 1-19.
- Thornton C. (2000) Numerical simulations of deviatoric shear deformation of granular media. *Géotechnique* 50, 43 53.
- Wichtmann T. et al. (2005) Strain accumulation in sand due to cyclic loading: drained triaxial tests. *Soil Dynamics and Earthquake Engineering* 25, 967 979.
- Wichtmann T. et al. (2007) Strain accumulation in sand due to cyclic loading: Drained cyclic tests with triaxial extension. *Soil Dynamics and Earthquake Engineering* 27, 42 48.
- Wood, D., ed. (1990), Soil Behaviour and Critical State Soil Mechanics, Cambridge University Press, Cambridge.